

DLGAN: Disentangling Label-Specific Fine-Grained Features for Image Manipulation

Guanqi Zhan* Yihao Zhao* Bingchan Zhao Haoqi Yuan Baoquan Chen Hao Dong
CFCS, Computer Science Dept., Peking University

Abstract

Several recent studies have shown how disentangling images into content and feature spaces can provide controllable image translation/manipulation. In this paper, we propose a framework to enable utilizing discrete multi-labels to control which features to be disentangled, i.e., disentangling label-specific fine-grained features for image manipulation (dubbed DLGAN). By mapping the discrete label-specific attribute features into a continuous prior distribution, we enable leveraging the advantages of both discrete labels and reference images to achieve image manipulation in a hybrid fashion. For example, given a face image dataset (e.g., CelebA) with multiple discrete fine-grained labels, we can learn to smoothly interpolate a face image between black hair and blond hair through reference images while immediately control the gender and age through discrete input labels. To the best of our knowledge, this is the first work to realize such a hybrid manipulation within a single model. Qualitative and quantitative experiments demonstrate the effectiveness of the proposed method.

1. Introduction

Image-to-image translation focuses on the use of the semantic visual information of a given image to conduct image synthesis. It has a wide range of applications, such as image super-resolution [19], image colorization [35], artwork synthesis [31], and photo-realistic image synthesis [32]. Pix2pix [14] achieves image-to-image translation on various datasets in a supervised setting, and CycleGAN [36] achieves the translation without requiring paired images for supervision.

To provide a more controllable synthesis, there are many works to manipulate/translate the input image by leveraging additional information, such as discrete labels [6], text descriptions [8], bash-based interfaces [2] and style images [12]. They enable users to manipulate the image in a different way. On the other hand, other works, such as

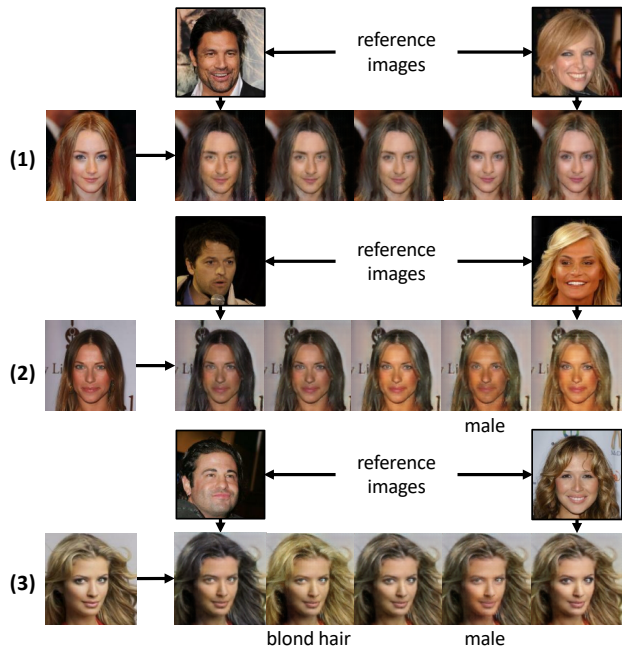


Figure 1. **Example results of DLGAN.** reference images control the *smooth manipulation* while discrete labels control the *immediate manipulation*; the labels take precedence over the reference images. The top row shows an example to smoothly manipulate the hair color and gender, while maintaining the other content information (e.g., the facial appearance and background).

DRIT [20] and MUNIT [13] disentangle the latent space of the image into a domain-invariant content space and a domain-specific attribute space. They can translate an image from one domain to another conditioned on the style of the reference image.

Different from those works, this paper focuses on leveraging the advantages of both fine-grained discrete labels and reference images to achieve *controllable* image manipulation. By first using the *discrete* fine-grained labels to control which features to be disentangled, and then mapping the *discrete* fine-grained features into a *continuous prior distribution*, as shown in Figure 1, we enable the *smooth linear*

*equal contribution

interpolation between the reference images. Meanwhile, additional labels can be used as a constraint to enable *immediate manipulation*, providing a hybrid and fine-grained way to manipulate images.

The main contribution of our work is an end-to-end method to support image manipulation conditioned on both images and labels, enabling both smooth and immediate changes. Experiments on CelebA [22] and DukeMTMC [30] datasets demonstrate the effectiveness of the proposed method. We call the proposed method as Disentangle Label GAN (DLGAN).

2. Related Work

Generative adversarial networks (GAN) learns to map one distribution to another distribution in a single feed-forward pass of a network [9] [15]. Conditional GAN is an important species of GAN that can generate images conditioned on input information. Prior works use conditioned GANs to synthesis images using different kinds of information, such as discrete labels [7, 27, 26], text captions [29, 34], and images [14].

Image-to-image translation is one type of conditional GAN that synthesizes images conditioned on the input images. Pix2pix [14] and BicycleGAN [37] achieve great success when paired images are accessible for training. There have also been works dealing with unpaired images, such as CycleGAN [36], DiscoGAN [16], and UNIT [21]. Image manipulation can be further controlled by additional auxiliary information, such as text caption [8], discrete label [6], style image [12], bash-based interface [2], and sparse annotation [28]. For multi-domain image-to-image translation, StarGAN [6] enables flexible translation for an image to any desired target domain with a label loss applied to the discriminator during the training process. In contrast to those works, we use GAN conditioned on both discrete labels and reference images for controllable image manipulation.

Feature disentanglement. Disentangling an image into different constituents requires modeling the factors of data variations. There have been early works disentangling images into class-related and class-independent components [18, 5, 25, 24]. As for unsupervised learning, InfoGAN [4] maximizes the mutual information between some latent variables and observation to achieve disentanglement. For unpaired data, DRIT [20], MUNIT [13], and EG-UNIT [23] decompose the image representation into a content feature space that is domain-invariant and a style space that captures domain-specific properties to achieve the translation of an image to another domain. Our work differs from all these works in disentangling the label-specific fine-grained features of images and makes the image manipulation controlled by both reference images and labels.

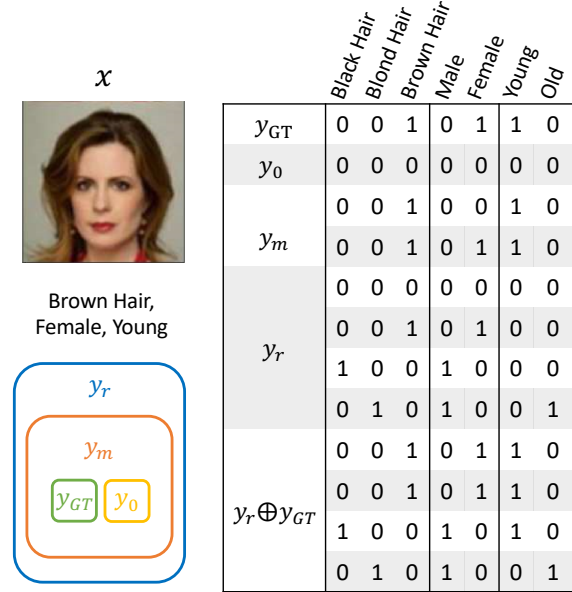


Figure 2. Example labels of a CelebA sample with the features of hair color, gender, and age. The relationships of different types of labels are shown in the Venn diagram on the bottom-left.

3. Method

Let $(\mathcal{X}, \mathcal{Y}) \subset (\mathbb{R}^{H \times W \times 3}, \mathbb{Y})$ be the space of a certain domain of images and labels, $x \in \mathcal{X}$ be an image sample and $y \in \mathcal{Y}$ be the corresponding discrete multi-labels that describe the fine-grained attributes of the image. The feature space of the image can be divided into two parts: 1) the label-specific attribute space A , which consists of the fine-grained features that the label y mentions, and 2) the content space C , which contains content features that the label y does not mention, such as the background and object shape.

Our goal is to use the discrete multi-labels to control which attribute features to be disentangled and map the attribute features into a continuous prior distribution. In doing so, we enable the smooth linear walk on the attribute space conditioned on reference images.

There are four networks in our model: an attribute encoder E_a , a content encoder E_c , a generator G , and a discriminator D . Their target can be viewed as four mappings in different spaces. The attribute encoder E_a maps images into the label-specific attribute space ($E_a : \mathcal{X} \rightarrow A$) and the content encoder E_c maps images into the content space ($E_c : \mathcal{X} \rightarrow C$). The generator G generates images conditioned on the content features, attribute features, and the input labels ($G : \{C, A, \mathcal{Y}\} \rightarrow \mathcal{X}$). The discriminator D aims to classify the input images into correct labels as well as to judge whether the images are realistic ($D : \mathcal{X} \rightarrow \{\{0, 1\}, \mathcal{Y}\}$, where the binary variable repre-

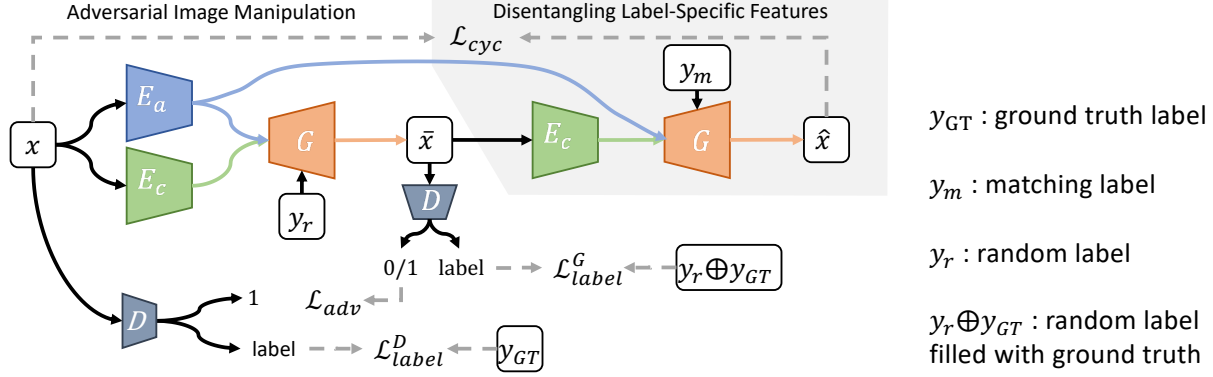


Figure 3. **The schematic overview of DLGAN.** The trapezoidal blocks with the same color indicate shared parameters. The area with a grey background is for label-specific feature disentanglement, while the other area is for image manipulation.

sents whether the image is real or fake).

In this section, we first illustrate our proposed fine-grained label representation in Section 3.1 and then discuss the strategies to manipulate the images and disentangle label-specific representations in Section 3.2 and 3.3. Finally, we detail the loss functions in Section 3.4.

3.1. Fine-Grained Label Representation

To achieve image manipulation and feature disentanglement, we define five different ways to represent the discrete fine-grained labels. An example of a certain image x is shown in Figure 2, where 1) y_{GT} denotes the ground-truth label where all feature information is provided, 2) y_0 denotes the empty label, which is a zero vector without feature information, 3) y_m denotes the matching label, where some of the ground truth features or even all of them are missing, and the remaining features must match the image, 4) y_r denotes the random label, which includes all possible combinations of the features and some or all features can be missing, and 5) $y_r \oplus y_{GT}$ denotes another type of random label where the missing features of y_r are filled with the ground truth features.

Concretely, take CelebA [22] as an example, if $\mathcal{Y} = \{\text{haircolor}, \text{gender}, \text{age}\}$, each label y can be represented by seven bits, where the first three bits represent the information of hair colors: “100”, “010”, and “001” indicate black, blond, and brown hair, respectively, and “000” means missing the information of hair color. The fourth and fifth bits represent the gender information, where “10” and “01” represent male and female, respectively, and “00” means missing the information of gender. Similarly, the last two bits represent the age information, where “10”, “01”, and “00” represent young, old, and unknown, respectively. As we mentioned, the random label y_r contains all possible cases of the feature combinations, and it has $36 = 4 \times 3 \times 3$ cases in this example. The matching label y_m is a subset of y_r , it has $8 = 2 \times 2 \times 2$ possible cases because each fea-

ture can be either missing or provided. For each one of the 36 cases of y_r , we fill the features of the ground truth label y_{GT} into the missing features of y_r to obtain the $y_r \oplus y_{GT}$. More examples of the label representation can be found in the supplementary.

The missing-feature property of y_m and y_r is important for the feature disentanglement. Details will be discussed in Section 3.3. Apart from disentanglement, the missing-feature property enables users to manipulate specific features of the image without providing the information of other features.

3.2. Adversarial Image Manipulation

To manipulate the image conditioned on the input labels, as the left of Figure 3 shows, the input image x is first fed into the content encoder E_c and the attribute encoder E_a . Then, the generator G first receives the representations of the input image from the encoders, and then learns to use a random label y_r to manipulate the input image by guiding the synthesized image $\bar{x} = G(E_c(x), E_a(x), y_r)$ to fool the discriminator D . Concretely, the discriminator learns to classify the real image x as real sample and classify the synthesized image \bar{x} as fake sample. The generator competes with the discriminator by learning to fool the discriminator to classify the synthesized images as real samples.

To stabilize the adversarial training process and generate higher-quality images, we use Wasserstein GAN [1, 10] adversarial loss with a gradient penalty as follows.

$$\begin{aligned}
 \mathcal{L}_{adv} = & -\mathbb{E}_{x, y_r} [D_{logit}(G(E_c(x), E_a(x), y_r))] \\
 & + \mathbb{E}_x [D_{logit}(x)] \\
 & - \lambda_{gp} \mathbb{E}_{\tilde{x}} [(||\nabla_{\tilde{x}} D_{logit}(\tilde{x})||_2 - 1)^2]
 \end{aligned} \tag{1}$$

where D_{logit} denotes the real/fake output of discriminator, λ_{gp} is the weight of the gradient penalty loss and \tilde{x} is sampled uniformly along a straight line between a pair of a real

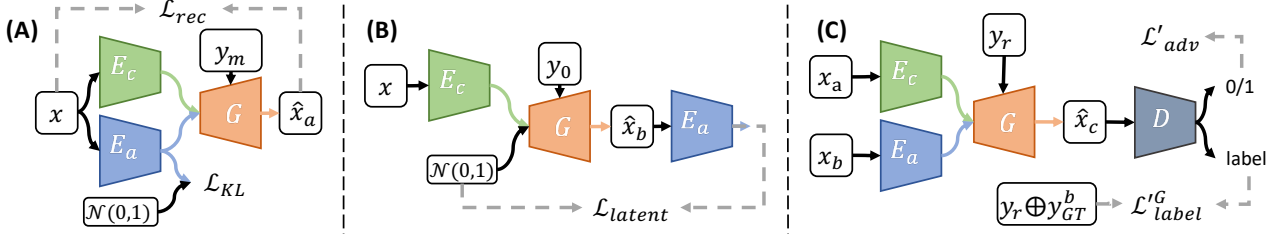


Figure 4. **Other regularization losses.** The identity reconstruction loss \mathcal{L}_{rec} facilitates the training and encourages the generator to maintain the background of the input image better; the KL loss \mathcal{L}_{KL} aims to align the attribute representation with a prior normal distribution; the latent regression loss \mathcal{L}_{latent} enforces the reconstruction on the latent attribute vector; and the additional adversarial loss \mathcal{L}'_{adv} and label loss \mathcal{L}'_{label} promote further feature disentanglement. The trapezoidal blocks with the same color indicate shared parameters with Figure 3.

and a synthesized image [1].

In addition, to ensure the synthesized images match with the input label, the discriminator learns to classify the real image x into the ground truth label y_{GT} . Meanwhile, the generator learns to synthesize image \bar{x} to match with the desired label $y_r \oplus y_{GT}$. In other words, if y_r has missing features, the synthesized image \bar{x} should maintain the corresponding original features of the input image x . To achieve that, two label losses are applied to the discriminator and generator, respectively:

$$\mathcal{L}_{label}^D = \mathbb{E}_x[\mathcal{CE}(D_{label}(x), y_{GT})] \quad (2)$$

$$\mathcal{L}_{label}^G = \mathbb{E}_{x, y_r}[\mathcal{CE}(D_{label}(\bar{x}), y_r \oplus y_{GT})], \quad (3)$$

where \mathcal{CE} stands for cross-entropy and D_{label} denotes the output label of discriminator.

3.3. Disentangling Label-Specific Features

We can now manipulate the input images using the random label y_r , but how to disentangle and map the label-specific features into a prior distribution? To achieve that, as the schematic indicated by the grey background in Figure 3 shows, we reconstruct the input image x by $\hat{x} = G(E_c(\bar{x}), E_a(x), y_m)$. The cycle-consistent loss \mathcal{L}_{cyc} between the input image x and reconstructed image \hat{x} guarantees that the output of the attribute encoder E_a contains the label-specific features. The reason is that by using a random label y_r to manipulate the input image x , the synthesized/manipulated image \bar{x} does not always contain all label-specific features of the original input image. At the same time, the matching label y_m also does not always contain all label-specific information of the original input image. In other words, both the $E_c(\bar{x})$ and y_m cannot provide all label-specific features of the input image for the \hat{x} . Therefore, to reconstruct the input image under different cases of y_r and y_m , all label-specific features of the input image x must be passed through the attribute encoder E_a .

The cycle-consistent loss is as follows.

$$\mathcal{L}_{cyc} = \mathbb{E}_x[||\hat{x} - x||_1], \quad (4)$$

The label representation method described in Section 3.1 plays an important role in our method. Specifically, the missing-feature property of y_m and y_r is necessary to achieve the disentanglement of label-specific representations. If y_m and y_r have no missing features, no label-specific feature needs to be passed through E_a . Then all features of the image can be passed through E_c , indicating a failure in disentanglement. In addition, the missing-feature property enables users to manipulate a specific feature of the image without being required to provide the information of other features.

Apart from the feature disentanglement, the cycle-consistent loss can “force” the manipulated image \bar{x} to maintain information (e.g., background) from the input image x ; otherwise, the reconstruction process cannot reconstruct the input images well [36]. In addition, as Part (A) of Figure 4 shows, we can further apply an identity reconstruction loss \mathcal{L}_{rec} to facilitate the training. Since the matching label y_m can be missing in some or all label-specific features, to reconstruct $\hat{x}_a = G(E_c(x), E_a(x), y_m)$, all image features, including label-specific and content features, must pass through the E_a and E_c . The identity reconstruction loss \mathcal{L}_{rec} is as follows.

$$\mathcal{L}_{rec} = \mathbb{E}_x[||\hat{x}_a - x||_1] \quad (5)$$

To support smooth manipulation, e.g., changing the hair color from one to another smoothly rather than by an immediate change, and to perform stochastic sampling, we need to map the attribute features into a prior normal distribution. To achieve that, the output of E_a is set to be a 1D vector, and we apply a KL-divergence loss between the output of E_a and the normal distribution $\mathcal{N}(0, 1)$, as shown in Part (A) of Figure 4. The KL-divergence loss \mathcal{L}_{KL} is as follows.

$$\mathcal{L}_{KL} = \mathbb{E}_x[\mathcal{D}_{KL}(E_a(x)||\mathcal{N}(0, 1))] \quad (6)$$

where $\mathcal{D}_{KL}(p||q) = -\int p(z)\log\frac{p(z)}{q(z)}dz$ denotes KL-divergence between two distributions.

3.4. Other Regularization

3.4.1 Latent Regression Loss

To encourage invertible mapping between the image space and the latent space, we can further apply an additional latent regression loss \mathcal{L}_{latent} [37]. As shown in Part (B) of Figure 4, we can sample a latent vector z from the prior normal distribution as the attribute representation and attempt to reconstruct z with $\hat{z} = E_a(\hat{x}_b)$, where $\hat{x}_b = G(E_c(x), z, y_0)$. The latent regression loss \mathcal{L}_{latent} can be formulated as follows.

$$\mathcal{L}_{latent} = \mathbb{E}_{x,z}[\|\hat{z} - z\|_1] \quad (7)$$

3.4.2 Additional Disentanglement Loss

In addition, Part (C) of Figure 4 can help to further disentangle the label-specific attribute features by guiding the generator to generate an image with content features and attribute features from two different images. The label loss for G in Part (C) is as follows.

$$\mathcal{L}_{label}^G = \mathbb{E}_{x_a, x_b, y_r}[\mathcal{CE}(D_{label}(\hat{x}_c), y_r \oplus y_{GT}^b)] \quad (8)$$

where $\hat{x}_c = G(E_c(x_a), E_a(x_b), y_r)$, and $y_r \oplus y_{GT}^b$ denotes a random label where the missing features of y_r are filled with the ground truth of the reference image x_b . \mathcal{L}_{label}^G can guide the generator to synthesize the images that match the attribute of the reference images and labels. The adversarial loss in Part (C) is as follows.

$$\mathcal{L}'_{adv} = -\mathbb{E}_{x_a, x_b, y_r}[D_{logit}(G(E_c(x_a), E_a(x_b), y_r))] \quad (9)$$

which is applied to the generator and reversely to the discriminator to encourage the generator to synthesize highly realistic images.

3.4.3 Total Loss

To conclude, the overall loss function for generator, content encoder, and attribute encoder is as follows.

$$\begin{aligned} \mathcal{L}_{Total}^{G, E_a, E_c} = & \lambda_{label}^G (\mathcal{L}_{label}^G + \mathcal{L}'_{label}^G) \\ & + (\mathcal{L}_{adv} + \mathcal{L}'_{adv}) \\ & + \lambda_{cyc} \mathcal{L}_{cyc} + \lambda_{rec} \mathcal{L}_{rec} \\ & + \lambda_{latent} \mathcal{L}_{latent} + \lambda_{KL} \mathcal{L}_{KL} \end{aligned} \quad (10)$$

The overall loss function for the discriminator is as follows.

$$\mathcal{L}_{Total}^D = -(\mathcal{L}_{adv} + \mathcal{L}'_{adv}) + \lambda_{label}^D \mathcal{L}_{label}^D \quad (11)$$

where the λ_{label}^G , λ_{cyc} , λ_{rec} , λ_{latent} , λ_{KL} , and λ_{label}^D are all scale values that control the weights of different losses.

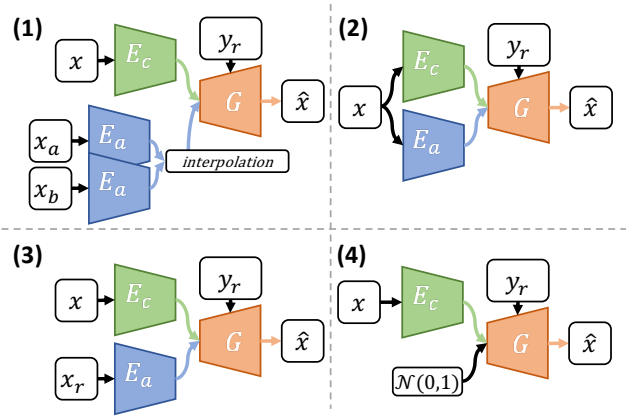


Figure 5. **Inferences for different applications.** (1) Manipulate the attributes of x by interpolating the attribute features of two reference images x_a and x_b while additional labels y_r can be used as a constraint. (2) Manipulate the image x 's attributes using label y_r only. (3) Manipulate the image x 's attributes using both label y_r and reference image x_r , where the y_r has higher priority than x_r . (4) Manipulate the image x 's attributes randomly while additional label y_r can be used as a constraint.

4. Experiment

4.1. Datasets and Implementation Details

We conduct two experiments on two multi-label datasets, CelebA [22] and DukeMTMC [30]. For CelebA, we use the labels of hair colors (black, blond, and brown), gender (male and female) and age (old and young). We use 100,000 images for training and 15,309 images for testing. For DukeMTMC, we choose to investigate into the colors of upper-body and lower-body clothing. We discard colors with samples fewer than 1,000, such as purple and green for upper-body and red and brown for lower-body. We use 11,643 images for training and 1,681 images for testing.

To represent the content information (*e.g.*, facial appearance and background) of the input image, the output of the content encoder is a 3D tensor which can contain more spatial information than 1D vector. Specifically, the content encoder comprises of two convolutional layers for down-sampling and three residual blocks [11]. For CelebA with the image size of 128×128 , the content encoder encodes images into tensors with a shape of $32 \times 32 \times 256$. For DukeMTMC with the image size of 64×128 , we use the same architecture, and the shape of content tensor becomes $16 \times 32 \times 256$. The attribute encoder comprises of three residual blocks to encode images into vectors with a dimension of 16. The generator comprises of six residual blocks followed by two deconvolutional layers for upsampling. We use the discriminator architecture of StarGAN to classify whether images are real or fake as well as classify them into their corresponding labels. We use batch normaliza-



Figure 6. **Example results of DLGAN on CelebA and DukeMTMC.** For both datasets, we conduct experiments on all the four applications. For DukeMTMC, labels are shown in two rows. The upper row represents the color of upper body clothing and the lower row represents the color of lower body clothing. “-” means empty label. More results can be seen in supplementary.

tion for the content encoder, attribute encoder and generator but layer normalization for the discriminator. For training, we adopt the verified settings of $\lambda_{cyc} = 10$, $\lambda_{KL} = 0.01$, $\lambda_{label}^D = 1$, $\lambda_{label}^G = 1$ and $\lambda_{gp} = 10$ according to the previous image manipulation studies [20, 6]. Besides, after trying a wide range of values for the rest of lambdas varying from 0.01 to 50, we empirically find that the fittest setting is $\lambda_{rec} = 1$ and $\lambda_{latent} = 5$. The same setting is used for both datasets. We use Adam optimizer [17] with a batch size of 32 and an initial learning rate of 0.0001. The model is trained for 20 epochs (on CelebA) and 200 epochs (on DukeMTMC), and the learning rate is linearly decayed to zero after half of the total epoch. The code is publicly available at <http://github.com/TBA> and the training on a V100 GPU took 5 days for CelebA and 3 days for DukeMTMC.

4.2. Qualitative Evaluation

Figure 5 shows the schematics of different applications of DLGAN. The results on the testing set for both datasets are in Figure 6. To demonstrate that DLGAN can walk on the manifold of the attribute feature space, *Application 1* uses the interpolation between the attribute features of two reference images as the new attribute representation for manipulation. Meanwhile, a non-empty label can be used as a constraint, e.g., as the top-left of Figure 6 shows, the interpolated images are controlled by the given label of female.

Application 2 provides a classic way to manipulate images conditioned on the given label only. In *Application 3*, a synthesized image \hat{x} is composed of the content of the input image x and the attributes of the reference image x_r and label y_r , where the label has a higher priority than the reference image. For *Application 4*, by using random normal noises $\mathcal{N}(0, 1)$ as the input attribute features, the generator

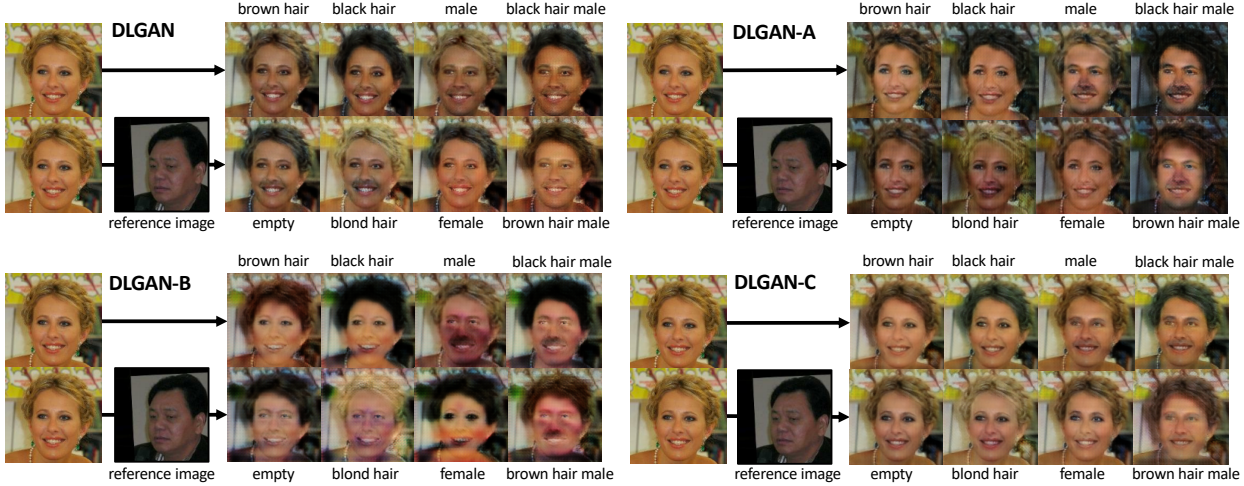


Figure 7. **The comparison of different DLGAN settings.** DLGAN-A has poorer performance than DLGAN in terms of maintaining the background of the input images. The results of DLGAN-B have artifacts (*e.g.*, spots and stripes) on people’s faces, which are not shown in the results of DLGAN. In some cases, the synthesized images of DLGAN-C cannot contain the attributes from the reference images x_r in *Application 3*.

can synthesize a series of images \hat{x} with the content identical to the input image x , meanwhile, an additional label y_r can be used as a constraint.

Applications 1 and 4 demonstrate that DLGAN successfully maps the discrete attributes into a continuous prior distribution. In addition, *Applications 2 and 3* can generate images with certain attributes, which will be used for the quantitative evaluation in Section 4.3. We analyze DLGAN by comparing four different settings: 1) DLGAN; 2) without Part (A) of Figure 3 and the corresponding $\mathcal{L}_{rec}, \mathcal{L}_{KL}$, namely DLGAN-A; 3) without Part (B) of Figure 3 and the corresponding \mathcal{L}_{latent} , namely DLGAN-B; and 4) without Part (C) of Figure 3 and the corresponding $\mathcal{L}'_{adv}, \mathcal{L}'_{label}$, namely DLGAN-C. This ablation study helps us analyze the effectiveness of our method.

Figure 7 shows some results of different DLGAN settings on CelebA dataset. The results of DLGAN-A demonstrate that, though the images are modified according to reference images and labels, DLGAN-A has poorer performance than DLGAN in terms of maintaining the background of the input images. The results of DLGAN-B have artifacts (*e.g.*, spots and stripes) on people’s faces, which are not shown in the results of DLGAN. In some cases, the synthesized images of DLGAN-C cannot contain the attributes from the reference images x_r in *Application 3*, *e.g.*, as shown in the lower row of DLGAN-C part of Figure 7 where the black hair attribute cannot be passed to the first and third synthesized images when input label is missing in hair color. The results indicate that DLGAN-C has a poor performance in feature disentanglement. More example results of DLGAN are provided in the supplementary

material.

4.3. Quantitative Evaluation

DLGAN-C, DLGAN-D, DLGAN-E and StarGAN are baseline models in our quantitative evaluation setting.

<i>Application2</i>	CelebA			DukeMTMC	
	hair	gender	age	down	up
DLGAN	14.61	18.74	15.23	84.94	91.91
DLGAN-A	32.36	38.96	34.71	101.98	106.51
DLGAN-B	38.01	43.82	43.15	115.35	119.05
DLGAN-C	16.50	26.26	19.88	97.74	105.77
StarGAN	12.69	18.12	14.02	101.83	105.95

<i>Application3</i>	CelebA			DukeMTMC	
	hair	gender	age	down	up
DLGAN	21.56	30.67	26.31	93.08	116.39
DLGAN-A	34.63	40.29	38.91	131.22	149.28
DLGAN-B	50.81	53.89	54.57	104.53	121.77
DLGAN-C	36.06	42.85	38.46	95.50	115.76

Table 1. The comparison of our method in different aspects using FID.

4.3.1 Fréchet Inception Distance

Fréchet Inception Distance (FID), a standard method to evaluate the distance between two distributions, has been widely used to evaluate the quality of the synthesized images [33, 3]. For quantitative evaluation, different methods manipulate all testing set images conditioned on the same random labels and reference images. Table 1 lists the FID

scores between the distribution of real images and generated images with respect to different attributes under different methods.

The results show that DLGAN outperforms other DLGAN settings on all attributes in both datasets for *Application 2*. Also, DLGAN achieves competitive results with the representative method, StarGAN, which is specifically designed for this application.

As StarGAN does not support *Application 3*, we only compare different DLGAN settings in *Application 3*. We also find that DLGAN performs better than other settings. The results in CelebA show the importance of the additional loss functions in Figure 4. For DukeMTMC dataset, DLGAN still performs competitively or better than other settings.

The FID score has limitation that it assumes features are of normal distribution, which is not guaranteed in real datasets, thus we further apply human evaluation.

<i>Application 2</i>	CelebA		DukeMTMC	
	a	b	a	b
DLGAN-A	1.86	1.33	1.41	1.89
DLGAN-B	2.19	2.04	1.83	2.65
DLGAN-C	1.14	1.07	1.41	1.76
StarGAN	0.85	0.94	1.16	1.23

<i>Application 3</i>	CelebA		DukeMTMC	
	a	b	a	b
DLGAN-A	2.59	1.63	3.17	2.98
DLGAN-B	13.10	2.52	2.24	3.11
DLGAN-C	2.34	2.01	1.52	2.61

Table 2. AMT perceptual evaluation of our method in different aspects. The numbers indicate the ratio of users who favor the results of DLGAN to users who favor a certain competing method. **a**: Realism. **b**: Correctness of the modified attributes.

4.3.2 Human Evaluation

To further evaluate our method, similar to previous studies [6, 36], we use Amazon Mechanical Turk (AMT) to compare the perceptual visual fidelity (*i.e.*, realism) and the correctness of the modified attribute features of our method against different baseline models. Specifically, we present the AMT workers with image pairs side by side on the screen. For each pair, one image is generated by DLGAN while the other image is generated by a randomly picked baseline model. To make the workers not know from which model the images are generated, the image positions are random in the pair, *i.e.*, the image generated by DLGAN on the left or right is of equal possibility.

We give unlimited time to the workers to make the selection. For fair comparison, we randomly generate 2,000 image pairs for CelebA and 1,000 image pairs for

DukeMTMC conditioned on randomly picked labels and reference images. For quality control, each image pair is compared by 5 different workers, and we only approve workers with a life-time task approval rate greater than 98% to participate in the evaluation. The workers are required to compare the image pairs based on the following criteria: a) Whether the synthesized image is realistic as well as maintaining the background and facial appearance in the original image. b) Whether the modified attributes are correct.

As shown in Figure 5, for *Application 2*, the criterion for correctness is that the modified image should correspond to the label $y_r \oplus y_{GT}$. For *Application 3*, the criterion for correctness is almost the same with the only difference that the target attributes become $y_r \oplus y_{GT}^b$, where the y_{GT}^b is from the reference image.

Table 2 shows the human evaluation results. The numbers in the table indicate the ratio of workers who favor the results of DLGAN to those who favor the results of competing methods. The ratio greater than one means that DLGAN has better performance than the competing method. Column “a” and “b” are the evaluations of realism and correctness of the modified attributes, respectively.

To summarize, the results of human evaluation conform to those of the machine evaluation explained above. For *Application 2*, even though StarGAN has slightly better performance than DLGAN on CelebA, DLGAN performs better than StarGAN on DukeMTMC and is able to support more applications. Besides, DLGAN outperforms other DLGAN settings in both *Application 2* and *Application 3* in both aspects, proving the effectiveness of our model.

5. Conclusions

In this paper, we propose a framework for disentangling the label-specific fine-grained features, enabling immediate manipulation by the discrete labels and smooth manipulation by the reference images within a single model. To our best knowledge, this is the first work to support such hybrid image manipulation for discrete multi-label datasets. In the future, we hope the proposed method can be generalized to different data modality.

References

- [1] Martin Arjovsky, Soumith Chintala, and Léon Bottou. Wasserstein generative adversarial networks. In *ICML*, 2017.
- [2] David Bau, Hendrik Strobelt, William Peebles, Jonas Wulff, Bolei Zhou, Jun-yan Zhu, and Antonio Torralba. Semantic photo manipulation with a generative image prior. In *SIGGRAPH*, 2019.
- [3] Andrew Brock, Jeff Donahue, and Karen Simonyan. Large scale gan training for high fidelity natural image synthesis. In *Proceedings of the International Conference on Learning Representations (ICLR)*, 2018.

- [4] Xi Chen, Yan Duan, Rein Houthoofd, John Schulman, Ilya Sutskever, and Pieter Abbeel. InfoGAN: Interpretable representation learning by information maximizing generative adversarial nets. In *NeurIPS*, 2016.
- [5] B. Cheung, J-A. Livezey, A-K. Bansal, and B-A Olshausen. Discovering hidden factors of variation in deep networks. In *ICLR*, 2015.
- [6] Yunjey Choi, Minje Choi, Munyoung Kim, Jung-Woo Ha, Sunghun Kim, and Jaegul Choo. Stargan: Unified generative adversarial networks for multi-domain image-to-image translation. In *CVPR*, 2018.
- [7] Emily Denton, Soumith Chintala, Arthur Szlam, and Rob Fergus. Deep generative image models using a laplacian pyramid of adversarial networks. In *NeurIPS*, 2015.
- [8] Hao Dong, Simiao Yu, Chao Wu, and Yike Guo. Semantic image synthesis via adversarial learning. In *ICCV*, 2017.
- [9] Ian Goodfellow, Jean Pouget-Abadie, Mehdi Mirza, Bing Xu, David Warde-Farley, Sherjil Ozair, Aaron Courville, and Yoshua Bengio. Generative adversarial nets. In *NeurIPS*, 2014.
- [10] Ishaan Gulrajani, Faruk Ahmed, Martin Arjovsky, Vincent Dumoulin, and Aaron Courville. Improved Training of Wasserstein GANs. In *NeurIPS*, 2017.
- [11] Kaiming He, Xiangyu Zhang, Shaoqing Ren, and Jian Sun. Deep residual learning for image recognition. In *CVPR*, 2016.
- [12] Xun Huang and Serge Belongie. Arbitrary style transfer in real-time with adaptive instance normalization. In *ICCV*, 2017.
- [13] Xun Huang, Ming-yu Liu, Serge Belongie, and Jan Kautz. Munit: Multimodal unsupervised image-to-image translation. In *ECCV*, 2018.
- [14] Phillip Isola, Jun-Yan Zhu, Tinghui Zhou, and Alexei A. Efros. Image-to-image translation with conditional adversarial networks. In *CVPR*, 2017.
- [15] Tero Karras, Samuli Laine, and Timo Aila. A style-based generator architecture for generative adversarial networks. In *CVPR*, 2019.
- [16] Taeksoo Kim, Moonsu Cha, Hyunsoo Kim, Jungkwon Lee, and Jiwon Kim. Learning to discover cross-domain relations with generative adversarial networks. In *ICML*, 2017.
- [17] Diederik Kingma and Jimmy Ba. Adam: A Method for Stochastic Optimization. In *ICLR*, 2014.
- [18] D.-P. Kingma, D. Rezende, S.-J. Mohamed, and M Welling. Semi-supervised learning with deep generative models. In *NeurIPS*, 2014.
- [19] Christian Ledig, Lucas Theis, Ferenc Huszar, Jose Caballero, Andrew Cunningham, Alejandro Acosta, Andrew Aitken, Alykhan Tejani, Johannes Totz, Zehan Wang, and Wenzhe Shi. Photo-realistic single image super-resolution using a generative adversarial network. In *CVPR*, 2017.
- [20] Hsin-Ying Lee, Hung-Yu Tseng, Qi Mao, Jia-Bin Huang, Yu-Ding Lu, Maneesh Singh, and Ming-Hsuan Yang. Dri++: Diverse image-to-image translation via disentangled representations. In *arXiv:1905.01270*, 2019.
- [21] Ming-Yu Liu, Thomas Breuel, and Jan Kautz. Unsupervised image-to-image translation networks. In *NeurIPS*, 2017.
- [22] Ziwei Liu, Ping Luo, Xiaogang Wang, and Xiaoou Tang. Deep learning face attributes in the wild. In *ICCV*, December 2015.
- [23] Liqian Ma, Xu Jia, Stamatios Georgioulis, Tinne Tuytelaars, and Luc-Van Gool. Exemplar Guided Unsupervised Image-to-Image Translation with Semantic Consistency. In *ICLR*, 2019.
- [24] A. Makhzani, J. Shlens, N. Jaitly, I. Goodfellow, and B Frey. Adversarial autoencoders. In *ICLR*, 2016.
- [25] M. Mathieu, J. Zhao, P. Sprechmann, A. Ramesh, and Y LeCun. Disentangling factors of variation in deep representation using adversarial training. In *NeurIPS*, 2016.
- [26] Mehdi Mirza and Simon Osindero. Conditional Generative Adversarial Nets. *arXiv preprint arXiv:1411.1784*, 2014.
- [27] Augustus Odena, Christopher Olah, and Jonathon Shlens. Conditional image synthesis with auxiliary classifier GANs. In *ICML*, 2017.
- [28] Scott Reed, Zeynep Akata, Santosh Mohan, Samuel Tenka, Bernt Schiele, and Honglak Lee. Learning what and where to draw. In *NeurIPS*, 2016.
- [29] Scott Reed, Zeynep Akata, Xinchun Yan, Lajanugen Logeswaran, Bernt Schiele, and Honglak Lee. Generative adversarial text to image synthesis. In *ICML*, 2016.
- [30] Ergys Ristani, Francesco Solera, Roger Zou, Rita Cucchiara, and Carlo Tomasi. Performance measures and a data set for multi-target, multi-camera tracking. In *ECCV*, 2016.
- [31] Matteo Tomei, Marcella Cornia, Lorenzo Baraldi, and Rita Cucchiara. Art2real : Unfolding the reality of artworks via semantically-aware image-to-image translation. In *CVPR*, 2019.
- [32] Ting-Chun Wang, Ming-Yu Liu, Jun-Yan Zhu, Andrew Tao, Jan Kautz, and Bryan Catanzaro. High-resolution image synthesis and semantic manipulation with conditional gans. In *CVPR*, 2018.
- [33] Taihong Xiao, Jiapeng Hong, and Jinwen Ma. Elegant: Exchanging latent encodings with gan for transferring multiple face attributes. In *ECCV*, 2018.
- [34] Han Zhang, Tao Xu, Hongsheng Li, Shaoting Zhang, Xiao lei Huang, Xiaogang Wang, and Dimitris Metaxas. StackGAN: Text to photo-realistic image synthesis with stacked generative adversarial networks. In *ICCV*, 2017.
- [35] Richard Zhang, Phillip Isola, and Alexei-A Efros. Colorful image colorization. In *ECCV*, 2016.
- [36] Jun-Yan Zhu, Taesung Park, Phillip Isola, and Alexei A. Efros. Unpaired image-to-image translation using cycle-consistent adversarial networks. In *ICCV*, 2017.
- [37] Jun-Yan Zhu, Richard Zhang, Deepak Pathak, Trevor Darrell, Alexei A. Efros, Oliver Wang, and Eli Shechtman. Toward multimodal image-to-image translation. In *NeurIPS*, 2017.